HHS Public Access

Author manuscript

Neuron. Author manuscript; available in PMC 2017 February 17.

Published in final edited form as:

Neuron. 2016 February 17; 89(4): 711–724. doi:10.1016/j.neuron.2016.01.004.

Rabies virus CVS-N2c$^{\Delta G}$ strain enhances retrograde synaptic transfer and neuronal viability

Thomas R. Reardon[1,*], **Andrew J. Murray**[1,5,*], **Gergely F. Turi**[2], **Christoph Wirblich**[4], **Katherine R. Croce**[1], **Matthias J. Schnell**[4], **Thomas M. Jessell**[1,3,†], and **Attila Losonczy**[2,3,†]

[1]Departments of Neuroscience and Biochemistry and Molecular Biophysics, Howard Hughes Medical Institute, Columbia University, New York, NY, 10032, USA

[2]Department of Neuroscience, Columbia University, New York, NY, 10032, USA

[3]Kavli Institute for Brain Science, Columbia University, New York, NY, 10032, USA

[4]Department of Microbiology and Immunology, Sidney Kimmel Medical College, Thomas Jefferson University, Philadelphia, PA, 19107, USA

Summary

Virally-based transsynaptic tracing technologies are powerful experimental tools for neuronal circuit mapping. The glycoprotein-deletion variant of the SAD-B19 vaccine strain rabies virus (RABV) has been the reagent of choice in monosynaptic tracing, since it permits the mapping of synaptic inputs to genetically marked neurons. Since its introduction, new helper viruses and reagents that facilitate complementation have enhanced the efficiency of SAD-B19$^{\Delta G}$ transsynaptic transfer, but there has been little focus on improvements to the core RABV strain. Here we generate a new deletion-mutant strain, CVS-N2c$^{\Delta G}$, and examine its neuronal toxicity and efficiency in directing retrograde transsynaptic transfer. We find that by comparison with SAD-B19$^{\Delta G}$, the CVS-N2c$^{\Delta G}$ strain exhibits a reduction in neuronal toxicity and a marked enhancement in transsynaptic neuronal transfer. We conclude that the CVS-N2c$^{\Delta G}$ strain provides a more effective means of mapping neuronal circuitry and of monitoring and manipulating neuronal activity *in vivo* in the mammalian central nervous system.

Correspondence to: AJM – ajm2199@columbia.edu, TMJ – tmj1@columbia.edu.

[5]Present address: Sainsbury Wellcome Centre for Neural Circuits and Behaviour, University College London, London, W1T 4JG. United Kingdom. a.murray@ucl.ac.uk

[*]These authors contributed equally to this work

[†]These authors contributed equally to this work

Author Contributions.

TRR, AJM, TMJ and AL conceived the project, designed the experiments and wrote the manuscript. TRR, AJM, GFT, AL and KRC performed experiments and analyzed the data. CW and MJS provided essential reagents, expertise, and input to the manuscript.

Introduction

The quest to understand the organization and function of neural circuits has been aided by the development of genetic techniques that link neuronal connectivity and animal behavior. Recombinant viruses have emerged as powerful tools for analyzing circuit structure and function (Nassi et al., 2015). When used with genetic markers for a large repertoire of neuronal types, recombinant transsynaptic viruses permit the construction of precise maps of synaptic input and output, and provide an entry point for identification and manipulation of targeted neurons. The efficacy of such viruses depends on three main features: selectivity of expression in pre-defined neuronal classes, long-term neuronal viability, and efficient marking of neuronal inputs or targets.

Rabies virus- (RABV) based techniques have achieved particular prominence in circuit mapping (Coulon et al., 1989, Ugolini, 2010) because they enable retrograde-, and for primary sensory neurons anterograde-, transsynaptic neuronal tracing (Ugolini, 1995; Zampieri et al., 2014). Moreover, the use of glycoprotein [G] deletion-mutant RABV$^{\Delta G}$ restricts viral budding and transfer, permitting selective mapping of first-order presynaptic neurons (Wickersham et al., 2007a,b). First-generation RABV$^{\Delta G}$ tools, based largely on the attenuated vaccine strain SAD-B19 (Schnell et al., 1994; Wickersham et al., 2007b), have two significant limitations: inefficiency of trans-synaptic transfer and neurotoxicity with longer-term infection (Schnell et al., 2009; Callaway and Luo, 2015; Ghanem and Conzelmann, 2015) (see schematic Figure 1A). Toxicity could reflect high levels of viral gene expression combined with inherent mechanisms for stabilizing viral glycoprotein (Morimoto et al., 2000; Palusa et al., 2012). Limitations to the efficiency of viral transfer could, in turn, be a function of weak viral neurotropism (Schnell et al., 2009; Conzelmann and Hagendorf, 2011). To address these limitations, we have explored whether the use of a different RABV strain might reduce toxicity and achieve improved transsynaptic transfer - permitting more accurate analysis of the organization of neural circuits in the mammalian central nervous system (CNS).

Many studies have documented laboratory RABV strains that exhibit varying degrees of pathogenicity. These strains range from virulent, highly neurotropic and neuroinvasive challenge viruses to apathogenic vaccine strains which have almost completely lost their neurotropism and neuroinvasiveness (Finke and Conzelmann, 2005; Jackson, 2013; Dietzschold et al., 2008). These laboratory strains exhibit predictable tropism and transmission speed, and are termed “fixed” viruses. The vaccine strain SAD-B19 was selected for its thermal stability, high titer in cell culture, low residual pathogenicity in small rodents and immunogenicity *in vivo* (Geue, et al., 2008) and was adopted as a neural circuit tracer (Kelly & Strick, 2000). In a search for alternative RABV strains, we focused our attention on “fixed” strains that have been selected for neuronal affinity and rapid transport *in vivo*, potentially making them better suited than vaccine strains for the analysis of neural circuitry. Amongst these fixed strains, the challenge virus CVS-N2c exhibits strong neurotropism and reduced cytotoxicity (Morimoto et al., 1998; Ugolini, 2010; Conzelmann and Hagendorf, 2011) and has been used previously, in a replication-competent form, for multisynaptic circuit mapping in primates (Hoshi et al., 2005). In addition, the availability of reverse-genetically rescued CVS-N2c (Wirblich and Schnell, 2011) enables the design of

replication-incompetent strains that can be rendered non-virulent and potentially more suitable for laboratory usage.

We report here the features of a glycoprotein-deficient CVS-N2c$^{\Delta G}$ strain derived from a virulent and highly neurotropic parental strain. Direct comparison with SAD-B19$^{\Delta G}$ reveals that CVS-N2c$^{\Delta G}$ exhibits lower levels of neurotoxicity and enhanced retrograde transsynaptic transfer. The enhanced efficacy of CVS-N2c$^{\Delta G}$ does not seem to be restricted to specific classes of neuron or circuits, in that we detected enhanced transsynaptic transfer in both corticostriatal and spinal premotor circuits. Neuronal viability is well maintained following infection by CVS-N2c$^{\Delta G}$ variants that express proteins that permit monitoring and manipulation of neurons, as demonstrated in the septo-hippocampal pathway and in the parabrachial projection to the ventral tegmental area (VTA). The new CVS-N2c$^{\Delta G}$ strain maintains compatibility with many of the helper viruses and complementation constructs used for SAD-B19, and thus constitutes a more effective reagent with which to probe the organization, physiology and behavioral relevance of neural circuits in the mammalian CNS.

Results

Recovery and pseudotyping of CVS-N2c$^{\Delta G}$

To provide a RABV strain for comparison with SAD-B19 derivatives, we explored the properties of a deletion mutant CVS-N2c strain, designated CVS-N2c$^{\Delta G}$, in which the glycoprotein gene (G) has been removed and complemented *in trans* by the deleted G gene, to permit retrograde monosynaptic transfer. The strong neurotropism of CVS-N2c may reflect the adaptation of virus to continued passage in mouse brain and cultured neuronal cell lines (Morimoto et al., 1998, 1999). We rescued and amplified virus exclusively in Neuro2A neuroblastoma cells, as a proxy for replication in primary neurons (see Experimental Procedures). Two Neuro2A-based lines were created for packaging: one expressing CVS-N2c(G) for use in amplification (Figure 1B), and the other expressing EnvA for use in pseudotyping (Figure 1C). To monitor viral transfer and neuronal viability, we created variants of CVS-N2c$^{\Delta G}$ expressing the fluorescent reporters dsRed or GFP (Figure 1B; Supplementary Figure 1). We noted that the maximum attainable titer of CVS-N2c$^{\Delta G}$ using our packaging cells was always lower than that achieved with SAD-B19$^{\Delta G}$ (Supplementary Table 1).

Enhanced transsynaptic transfer of CVS-N2c$^{\Delta G}$ virus

We compared the efficiency of retrograde monosynaptic transfer of the CVS-N2c$^{\Delta G}$ and SAD-B19$^{\Delta G}$ strains under similar infection conditions in cortico-striatal and spinal premotor circuits, assessing the spread of these viruses from primary infected, to transsynaptically-infected secondary neurons.

To achieve selective monosynaptic RABV transfer we used two priming (helper) reagents introduced *in trans*, one to complement the deleted RABV glycoprotein (G) gene and the other to express the pseudotyping receptor TVA. To induce complementation, we developed Cre-conditional adeno-associated viruses (AAV) expressing RABV(G) and a nuclear marker, human histone2B-GFP (nGFP) (Kanda et al., 1998; Sun et al., 2014). Two versions

of the virus, designated AAV-FLEX-nGFP-2A-RABV[G], were used to express either SAD-B19(G) or CVS-N2c(G) – proteins identical in length but differing in 60 amino acid residues. After Cre recombination, both viruses directed glycoprotein expression to similar levels, assessed by immunofluorescence (Supplementary Figure 2). Selectivity was established by targeting neuronal subtypes for EnvA/TVA pseudotyped RABV$^{\Delta G}$ infection (Wickersham et al., 2007b) using a Cre-conditional virus, AAV-FLEX-TVA-mCherry, to achieve TVA receptor expression (Watabe-Uchida et al., 2012).

To provide a background control we injected all viruses into wild-type mice and assayed non-targeted expression. Neither of the AAV-FLEX-nGFP-2A-RABV[G] variants exhibited spontaneous recombination or expression, as revealed by complete absence of nGFP^{+} neurons. We detected little to no “leaky” expression of TVA from our AAV-FLEX-TVA-mCherry, as revealed by the detection of <5 RFP^{+} neurons after over-infection with either RABV$^{\Delta G}$-dsRed[EnvA] virus, indicating that EnvA/TVA infections were highly selective. As a final control, a separate injection of EnvA-pseudotyped CVS-N2c$^{\Delta G}$ into the spinal cord resulted in a maximum of one infected neuron per animal, supporting the selectivity of infection (for viral controls see Experimental Procedures).

To assess transsynaptic transfer efficiency, neuronal infection with a mixture of the TVA and RABV(G) priming viruses (Figure 2A–C) was followed two weeks later by injection of matching EnvA-pseudotyped RABV$^{\Delta G}$-dsRed, either SAD-B19$^{\Delta G}$ or CVS-N2c$^{\Delta G}$. We used the maximum attainable titer for both the SAD-B19$^{\Delta G}$ and CVS-N2c$^{\Delta G}$ strains (Supplementary Table 1). Primary neurons were defined by co-expression of nGFP from RABV(G) priming virus and dsRed driven by RABV$^{\Delta G}$, whereas transsynaptically infected secondary neurons expressed dsRed alone. After an additional 10 days post-infection, primary and secondary neurons were counted and the extent of transfer determined from the ratio of secondary to primary infection numbers.

In the corticostriatal pathway, medium spiny neurons (MSN) of the striatum receive extensive excitatory input from cortical projection neurons (Gerfen and Bolam, 2010), prompting us to compare the degree of retrograde transsynaptic transfer from striatal to cortical neurons. To restrict priming infection we used mice expressing Cre-recombinase under the control of an *adenosine receptor 2A* (Adora2A) promoter, which is active in approximately half of all MSNs (Gong et al., 2007) (Figure 2B,C). In each animal, we counted all primary labeled neurons and sampled secondary labeled neurons from the same five cortical regions. For both RABV$^{\Delta G}$ strains we observed a relatively linear increase in transfer ratio as the number of primary neurons increased (primary/secondary neuronal numbers: CVS-N2c$^{\Delta G}$: 34/434, 57/810, 126/1240; SAD-B19$^{\Delta G}$: 126/44, 132/58, 450/400). These transfer counts indicate that CVS-N2c$^{\Delta G}$ virus exhibits a 22-fold higher (range 11- to 40-fold) incidence of retrograde transsynaptic transfer into cortical projection neurons than SAD-B19$^{\Delta G}$ virus (Figure 2D–F).

MSNs represent a near-homogenous and densely interconnected neuronal population, such that local intra-striatal transfer of RABV is expected. But in this circuit the determination of local viral transfer with current methods is not possible, for two reasons. First, TVA-mCherry is not detectable with native fluorescence (Watabe-Uchida et al., 2012; Krashes et

al., 2014). Nevertheless, antibody amplification of the mCherry signal will likely cross-react with RABV encoded dsRed, making primary vs secondary neuron identification ambiguous. Second, and more importantly, direct and transsynaptic infection by RABV$^{\Delta G}$ cannot be distinguished within the population of TVA-expressing striatal cells, making secondary infection counts unreliable.

This problem led us to evaluate the efficiency of transsynaptic viral transfer in a spinal circuit within which local transfer can be cleanly assayed, permitting the analysis of viral transfer as a function of axonal projection distance. We focused on spinal premotor circuits, where primary infected motor neurons transfer virus to premotor interneurons. Since motor neurons are anatomically and genetically distinguishable from surrounding spinal interneurons, the use of selective Cre mouse lines makes it possible to distinguish primary EnvA/TVA labeled motor neurons from both local and distant secondary transsynaptically-infected interneurons.

To target spinal motor neurons we used mice expressing Cre under control of the *choline acetyltransferase* (ChAT) promoter. Paired TVA and RABV(G) priming viruses were injected into the ventral horn of L3 and L4 lumbar spinal segments, followed two weeks later by L3 and L4 injection of RABV$^{\Delta G}$-dsRed[EnvA] (Figure 3A). Primary infection was limited to motor neurons, as identified by their distinct morphology and ventral position and nuclear expression of GFP by RABV(G) priming virus. We compared the total number of secondary infected neurons as a function of primary starter cell number for each strain, and found that SAD-B19$^{\Delta G}$ was transferred to 7.0 ± 0.5 secondary cells (mean ± s.e.m; Figure 3E), a number comparable to that found in previous studies using related helper viruses (Watabe-Uchida et al., 2012; Sun et al., 2014; Pollak Dorocic et al., 2014; Ogawa et al., 2014). By comparison, each CVS-N2c$^{\Delta G}$ primary neuron yielded 60.2 ± 16.3 secondary neurons (Figure 3E), close to an order of magnitude increase in the efficiency of total transsynaptic transfer.

We also analyzed the transfer ratio as a function of the distance of secondary neurons from the injection site. At local lumbar levels, we detected a ~80% reduction in primary infection by CVS-N2c$^{\Delta G}$ compared to SAD-B19$^{\Delta G}$, likely a result of the lower initial CVS-N2c$^{\Delta G}$ titer (Figure 3B,E,F, Supplementary Table 1). Despite this difference, the total number of secondary infected neurons detected at local lumbar levels was similar with both viral strains (Figure 3B,F), indicative of a ~4 fold enhancement from CVS-N2c$^{\Delta G}$ mediated local transsynaptic transfer. But for more distant interneurons found in thoracic and cervical spinal cord segments and in the hindbrain, pairwise comparison revealed a 16- to 50-fold enhancement in efficiency of CVS-N2c$^{\Delta G}$- over SAD-B19$^{\Delta G}$-mediated transfer (Figure 3C,D,G).

Thus, transsynaptic transfer of the CVS-N2c$^{\Delta G}$ strain exhibits an order of magnitude enhancement over SAD-B19$^{\Delta G}$, and an especially strong improvement in transfer efficacy into spinal premotor neurons with distant somata.

Restricted transsynaptic transfer of CVS-N2c$^{\Delta G}$

Resolving whether the transfer of CVS-N2c$^{\Delta G}$ is restricted to transsynaptic means is critical to the interpretation of anatomical tracing and connectivity maps. One report offered some evidence of synaptically restricted spread for SAD-B19 (Wickersham et al., 2007b). But the lack of conclusive evidence that any RABV strain is transferred exclusively across synapses makes it crucial to resolve whether CVS-N2c virus spreads by additional, non-synaptic, means.

We tested the exclusivity of CVS-N2c transfer at proprioceptive sensory synapses with spinal motor neurons, given that information on the normal pattern of connectivity in this circuit is available at high enough resolution to match experimental data with predictions about the selectivity of viral transfer. Within this circuit, proprioceptive sensory afferents make direct connections with spinal motor neurons that project to the same muscle (forming homonymous connections) and weaker connections to motor neurons innervating muscles with synergistic functions, termed heteronomous connections (Mendelsohn et al., 2015; Frank and Westerfield, 1983). In addition, despite the proximity of sensory terminals and motor neuron dendrites, proprioceptive sensory neurons do not form direct connections with motor neurons that innervate antagonistic muscles (Figure 4A,B; Eccles et al., 1957; Frank and Westerfield, 1983; Hongo et al., 1984; Mendelsohn et al., 2015). The conservation of sensory-motor synaptic selectivity across mammalian species provided the basis for a ‘homonymous vs antagonist’ assay to test the exclusivity of synaptic viral transfer in mice.

To examine the exclusivity of CVS-N2c$^{\Delta G}$ transfer we examined sensory-motor connectivity between ankle extensor gastrocnemius [GS] and ankle flexor tibialis anterior [TA] antagonist circuits. Motor neurons that innervate these two muscle groups possess dendrites that are interleaved in the ventral spinal cord (Figure 4B), permitting the detection of potential non-synaptic routes of transfer. We injected paired TVA and CVS-N2c(G) priming viruses into the GS muscle of *ChAT*-Cre mice, directing CVS-N2c(G) and TVA expression selectively in GS motor neurons (Figure 4C). Two weeks later EnvA-pseudotyped CVS-N2c$^{\Delta G}$-dsRed was injected into spinal segments L3–L6, selectively infecting GS motor neurons. We then examined the pattern of fluorescent protein labeling in peripheral sensory endings derived from homonymous GS and antagonist TA group Ia proprioceptive sensory afferents.

We detected dsRed-labeled sensory endings in contact with intrafusal muscle spindle fibers in 75% of GS muscles, but did not observe any dsRed-labeled spindle-associated sensory endings in the TA muscle (4 mice, n = 8 muscles; Figure 4D,E). This finding implies a tightly controlled and exclusively synaptic process of CVS-N2c$^{\Delta G}$ transfer from motor neurons to sensory terminals that form monosynaptic contacts with their target motor neuron pool.

Reduced expression and neurotoxicity of CVS-N2c$^{\Delta G}$ virus *in vitro*

To characterize CVS-N2c$^{\Delta G}$ for use in functional experiments we examined the level of RABV gene expression elicited by the SAD-B19$^{\Delta G}$ and CVS-N2c$^{\Delta G}$ strains. Neuro2A cells were infected with RABV$^{\Delta G}$-GFP, under conditions in which the multiplicity of infection

(MOI) was kept below 0.1, to avoid cellular infection by multiple copies of virus. Two days after infection, both RABV$^{\Delta G}$ strains directed GFP expression at similar levels; but after four days, the level of GFP expression directed by SAD-B19$^{\Delta G}$ was significantly higher than that conferred by CVS-N2c$^{\Delta G}$ (unpaired Student's t-test; $p = 0.045$, Figure 5A–C).

We next examined whether the SAD-B19$^{\Delta G}$ and CVS-N2c$^{\Delta G}$ strains differed in their ability to impose cytotoxic damage to Neuro2A cells. To assess this, we monitored the incidence of incorporation of propidium iodide (PI), a cell-impermeable DNA intercalating agent that is passively transferred through the plasma membrane of dead or dying cells. In uninfected Neuro2A cells, PI labeled 21% of cells, and in Neuro2A cells infected with CVS-N2c$^{\Delta G}$-GFP 22% of cells were PI labeled. But for Neuro2A cells infected with SAD-B19$^{\Delta G}$-GFP, 49% were PI labeled (Figure 5D–F) ($p = 0.037$, unpaired Student's t-test). Thus, SAD-B19$^{\Delta G}$ exerts a greater toxicity *in vitro* than CVS-N2c$^{\Delta G}$ strain, even with a comparatively inert fluorophore.

Manipulating and monitoring neural activity with CVS-N2c$^{\Delta G}$ virus

We next compared CVS-N2c$^{\Delta G}$ and SAD-B19$^{\Delta G}$ strains for their ability to express proteins to monitor and manipulate neuronal activity. To achieve this, we created RABV$^{\Delta G}$ variants expressing humanized channelrhodopsin2 (hChR2), or a genetically encoded calcium indicator, GCaMP6f (Zhang et al., 2006; Chen et al., 2013). In this set of experiments we controlled the duration of infection by injecting native-envelope RABV$^{\Delta G}$ viruses such that they directly infected the terminals of projection neurons in corticostriatal and hippocampal-septal circuits.

To explore the utility of SAD-B19$^{\Delta G}$ and CVS-N2c$^{\Delta G}$ as vectors for manipulating neural activity through hChR2 expression (Zhang et al., 2006) we first analyzed levels of neurotoxicity for each strain. Injection of RABV$^{\Delta G}$ into the dorsal striatum resulted in retrograde infection of cortical projection neurons. After 6 days, SAD-B19$^{\Delta G}$-hChR2-YFP infected neurons exhibited an aberrant neuronal morphology with distal dendrites exhibiting noticeable disruption, and the surrounding neuropil containing neuronal debris (Figure 6A,C). In contrast, near-normal cortical neuronal morphology was observed 6 days after infection with CVS-N2c$^{\Delta G}$-hChR2-YFP (Figure 6B,C).

We examined the ability of RABV$^{\Delta G}$-hChR2-YFP expression, to confer photoexcitability, assaying responses over a four-week period (Figure 6D,E,F). Using SAD-B19$^{\Delta G}$-hChR2-YFP virus, we detected few fully intact cortical neurons after 7 days of infection, precluding physiological analysis (6 animals; Figure 6A; data not shown). In contrast, photo-illumination at 473 nm wavelength of cortical neurons infected by CVS-N2c$^{\Delta G}$-hChR2-YFP reliably elicited action potentials in infected cortical neurons in acute forebrain slices (Figure 6E,F), for up to 28 days after infection. Spike frequency increased with the duration of viral expression over the first 10 days (Figure 6F,G). Moreover, recordings from nearby YFP^{off} uninfected cortical neurons revealed excitatory postsynaptic currents elicited by presynaptic photostimulation (Figure 6H). Stable whole-cell recordings from CVS-N2c$^{\Delta G}$-infected cortical neurons were obtained at a rate similar to that of uninfected neurons. Resting potentials (V_m) for infected and uninfected cells in the same animal were statistically similar over the infection period (−58.7mV ± 2.2, n = 7 versus −56.8mV ± 1.5, n

= 16); without a clear trend for changes in V_m as a function of infection time. These results document the efficacy of CVS-N2c$^{\Delta G}$ in expressing hChR2 under conditions that permit optogenetic manipulation of neuronal activity.

We next assessed the efficacy of CVS-N2c$^{\Delta G}$ and SAD-B19$^{\Delta G}$ as monitors of neural activity through expression of GCaMP6f (Chen et al., 2013). In this analysis we focused on hippocampal-septal circuits in which locomotion evokes robust hippocampal neuronal activity (Somogyi and Klausberger, 2008; Jinno et al., 2007). We first assayed neurotoxicity of each RABV$^{\Delta G}$ strain. Following injection of SAD-B19$^{\Delta G}$-GCaMP6f virus into the medial septum, infected hippocampal projection neurons exhibited marked signs of degeneration, most notably pronounced blebbing of neuronal processes 10 days after infection (Figure 7A,C). In contrast, septal neurons infected with CVS-N2c$^{\Delta G}$-GCaMP6f for one week exhibited near-normal morphology and only a modest disruption at two weeks (Figure 7B,C).

The activity of hippocampal-septal projection neurons after retrograde infection with CVS-N2c$^{\Delta G}$-GCaMP6f was determined through *in vivo* two-photon Ca^{2+} imaging (Figure 7E). We detected hippocampal neuronal GCaMP6f-Ca^{2+} transients in mice during treadmill locomotion, with a tight temporal coincidence in locomotor episodes and neuronal burst activity (Lovett-Barron et al., 2014) (Figure 7G). In addition, we found that the magnitude of treadmill based locomotion-evoked Ca^{2+} signals recorded from hippocampal-septal projection neurons was constant over the first two post-injection weeks (Figure 7F). Repeated recordings from identified neurons were possible for the entire usable duration of the cranial imaging window, at least 17 days post-infection. These findings establish that CVS-N2c$^{\Delta G}$ confers durable, and physiologically non-disruptive, expression of GCaMP6f, permitting analysis of neuronal activity *in vivo* for at least several weeks.

CVS-N2c expression level is sufficient to direct transgene recombination

CVS-N2c$^{\Delta G}$ infection directs comparatively low levels of gene expression, and thus it is unclear whether Cre or Flpo proteins can be expressed at concentrations sufficient to exert efficient enzyme-mediated recombination. To address this issue we constructed-mCherry-2A-Flpo and -mCherry-2A-Cre driver viruses for CVS-N2c$^{\Delta G}$ transduction. CVS-N2c$^{\Delta G}$-mCherry-2A-Flpo virus was injected into the lumbar spinal cord of mice harboring a Flp-GFP reporter (Figure 8A) and the incidence of retrogradely-infected neurons was examined in thoracic spinal cord. Germ-line expression of GFP served as an indicator of recombination, and was detected in all neurons infected with CVS-N2c$^{\Delta G}$-mCherry-2A-Flpo, revealed by expression of mCherry (Figure 8B). Thus, the level of Flpo expression achieved with CVS-N2c$^{\Delta G}$ transduction is sufficient to direct target gene recombination in an efficient manner.

In a similar manner, we investigated whether CVS-N2c$^{\Delta G}$ directs Cre-mediated recombination. We injected CVS-N2c$^{\Delta G}$-mCherry-2A-Cre into the ventral tegmental area (VTA) of wild type mice, and in parallel injected a Cre-conditional AAV expressing GFP (AAV-FLEX-GFP) into the parabrachial nucleus (PBN) (Figure 8C). We found that ~50% of mCherry^{+} RABV-infected neurons expressed GFP (Figure 8D), consistent with the sparsity of infection of PBN neurons and indicative of the efficacy of Cre expression.

Together, these collected observations document that CVS-N2c$^{\Delta G}$ rabies strain provides a more effective reagent than SAD-B19$^{\Delta G}$ when probing the organization and function of neural circuits in mouse brain and spinal cord (Table 1).

Discussion

Recombinant viruses facilitate the anatomical and functional analysis of mammalian neural circuits. We have explored the features of a recombinant strain of rabies virus, CVS-N2c$^{\Delta G}$, which permits monosynaptic tracing from genetically-defined neurons, as with the widely-used SAD-B19$^{\Delta G}$ strain. CVS-N2c$^{\Delta G}$ exhibits a marked reduction in neurotoxicity, both *in vitro* and *in vivo*, facilitating its application in monitoring and manipulating neural circuits. Moreover, direct comparison of CVS-N2c$^{\Delta G}$ and existing SAD-B19$^{\Delta G}$ strains reveals that CVS-N2c$^{\Delta G}$ provides at least an order of magnitude enhancement in transsynaptic transfer to presynaptic neurons, with an even greater enhancement in transfer to long-range inputs (Table 1). CVS-N2c-based tools may therefore enable access to circuits that have so far proven refractory to RABV interrogation.

Enhanced transsynaptic tracing with CVS-N2c$^{\Delta G}$

Two major drawbacks in the application of attenuated RABV-based tools are high neurotoxicity (Morimoto et al., 1999) and inefficiency of transsynaptic transfer (Callaway and Luo, 2015). Early generations of monosynaptic RABV-based vectors were primarily variants of the attenuated vaccine strain SAD-B19 (Schnell et al., 1994; Callaway and Luo, 2015; Ghanem and Conzelmann, 2015; Wickersham et al., 2007a,b), which is weakly neurotropic and strongly immunogenic. By contrast, most virulent RABV strains are highly neurotropic, neuroinvasive and, somewhat counter-intuitively, exhibit reduced immunogenicity and neurotoxicity by virtue of their sequestration in neurons and evasion of surveillance by immune cells (Schnell et al., 2009).

The contrasting features of the SAD-B19 and CVS-N2c strains may stem from differences in growth and selection conditions. SAD-B19 was developed as a vaccine vector through serial passaging on non-neuronal cells. In contrast, CVS-N2c was developed through exclusive passaging in neonatal mouse brain and murine neuroblastoma cells as a challenge virus for testing RABV vaccines (Morimoto et al., 1998). As a result CVS-N2c is highly neuroinvasive, has selective tropism for neuronal cells, lower replication and protein expression, and faster transport through the CNS (Bostan et al., 2010). These traits diverge from those of SAD-B19, which has a lower tropism for neurons, but a higher affinity for non-neuronal cells and faster replication. The consequence of accelerated replication is a greater number of viral particles and a strong induced immune response (see Schnell et al., 2009; Ghanem and Conzelmann, 2015; Morimoto et al., 1998 and Morimoto et al., 1999 for discussion on relative tropism and virulence of different RABV strains). These observations led us to consider whether a more virulent RABV strain might hold promise for circuit analysis. In addition, the reverse genetic rescue of the virulent CVS-N2c strain (Wirblich and Schnell, 2011) has eased the task of generating a glycoprotein deficient virus for use in monosynaptic tracing, as well as evading the biohazards inherent in working with virulent RABV.

We also provide evidence that CVS-N2c$^{\Delta G}$ is transferred retrogradely through an exclusive transsynaptic route. The analysis of sensory-motor connectivity shows that CVS-N2c$^{\Delta G}$ does not transfer to nearby, non-connected, synapses – with the implication that the enhancement in secondary neuron labeling occurs via an increase in synaptic transfer, rather than adventitious viral infection. The strength of glycoprotein complementation vector (Callaway and Luo, 2015), increased viral budding (Mebastion et al., 1996), enhanced glycoprotein neurotropism, reduced immunogenicity, and reduced viral toxicity (Schnell et al., 2009) may, separately or together, underlie the efficiency of RABV transfer and expression.

Of these variables, an increased neurotropism that maps to the viral glycoprotein is a plausible explanation for the increased transfer efficiency of CVS-N2c (Morimoto et al., 1998). We and others have replaced the SAD-B19 glycoprotein with that of CVS-N2c when complementing SAD-B19$^{\Delta G}$ virus and found that it increases transsynaptic transfer, although not to the levels observed with fully complemented CVS-N2c$^{\Delta G}$ virus (Kaifosh et al. 2013; Velez-Fort et al., 2014; Reardon, Murray, Jessell, and Losonczy, unpublished data). By implication, the CVS-N2c glycoprotein may enhance transsynaptic viral transfer. After CVS-N2c$^{\Delta G}$ infection the lack of infiltrating T-cells, antibodies and other antiviral immune effectors (Roy and Hooper, 2008; Schnell et al., 2009) may also increase the efficiency of viral transfer through the CNS. Finally, neuronal viability could extend the duration of competence for transsynaptic transfer, as well as maintain host accessory proteins that assist in RABV transfer. We note that our work relies on the same complementation strategy as Wickersham et al, (2007b), and thus any improvements to that system, such as enhancement in TVA/EnvA selectivity or glycoprotein expression vectors, can easily be applied to the CVS-N2c strain.

Selection of appropriate RABV vectors for circuit analysis

In our studies, CVS-N2c$^{\Delta G}$ showed at least an order of magnitude enhancement in transsynaptic spread compared to the SAD-B19$^{\Delta G}$ strain, and was particularly effective in transsynaptic infection of neurons with long-range projections. A similar improvement was seen in two distinct CNS circuits, suggesting that CVS-N2c$^{\Delta G}$ lacks neuronal subtype constraints as a transsynaptic tracer. Thus for anatomical studies CVS-N2c$^{\Delta G}$ appears to have major advantages over SAD-B19$^{\Delta G}$ and other prominent vaccine strains (Mori and Morimoto, 2014). Although it is conceivable that the transsynaptic efficiency of SAD-B19 could be improved with modifications to the complementation vectors (eg. DeNardo et al., 2015) or the use of alternate complementation methods (Rancz et al., 2011; Wertz et al., 2015) it is highly likely that the spread of CVS-N2c could be improved in the same way. Thus the use of the CVS-N2c$^{\Delta G}$ viral strain for anatomical studies has the potential to uncover aspects of neuronal connectivity inaccessible through the use of SAD-B19$^{\Delta G}$.

The ability to manipulate and monitor the activity of neurons within large networks, on behaviorally relevant timescales, sets CVS-N2c$^{\Delta G}$ apart from currently available RABV vectors. CVS-N2c$^{\Delta G}$ can drive tolerated levels of optogenetic activators, as well as recombinase proteins for selective recombination in presynaptic cells – opening the way for application of the full repertoire of conditional genetic tools in behaving animals. Previous

studies have expressed optogenetic and recombinase proteins via SAD-B19$^{\Delta G}$ strains (Osakada et al., 2011) but neuronal manipulations were typically restricted to short post-infection times, typically 5–7 days (Kiritani et al., 2012; Namburi et al., 2015).

We have found that use of SAD-B19$^{\Delta G}$ precludes functional analysis of neuronal activity, as a consequence of premature neuronal dysfunction or death. The high levels of protein expression achieved by SAD-B19$^{\Delta G}$ may be a major contributor to its viral toxicity (Morimoto et al., 1999; Morimoto et al., 2000; Schnell et al., 2009). In particular, high expression levels of optogenetic proteins may facilitate cell death faster than would be observed when SAD-B19$^{\Delta G}$ is used to express relatively inert fluorescent proteins (Lin, 2011; Cetin and Callaway, 2014). In contrast, CVS-N2c$^{\Delta G}$ permits viable expression and long-term functional analysis using GCaMP6f or hChR2. Indeed, GCaMP calcium transients were detectable in hippocampo-septal neurons for up to 17 days, and cortical neurons expressing hChR2 under CVS-N2c$^{\Delta G}$ control maintained normal cell physiology and functional responses for 28 days after infection. We cannot exclude that over longer post-infection times, CVS-N2c$^{\Delta G}$ may also induce neuronal dysfunction (Scott et al., 2008), but the existing time-window opens potential new avenues for functional and behavioral experiments not available through use of SAD-B19$^{\Delta G}$.

CVS-N2c$^{\Delta G}$ seems to have major advantages over SAD-B19$^{\Delta G}$ in terms of anatomical tracing and functional analysis of circuit organization. But there are circumstances whereby SAD-B19$^{\Delta G}$ remains a relevant reagent. The higher protein levels produced after SAD-B19$^{\Delta G}$ infection make it more suitable for use as an acute vector, when fast expression of the transgene is important. SAD-B19$^{\Delta G}$ drives protein expression just one day post-infection, which is not achievable with CVS-N2c$^{\Delta G}$. In addition, the higher SAD-B19$^{\Delta G}$ directed protein expression levels permit visualization of fine neuronal morphologies (Wickersham et al. 2007a,b).

Moreover, the generation of viral particles in the laboratory is currently easier with SAD-B19$^{\Delta G}$ than with CVS-N2c$^{\Delta G}$. Titers on the order of 1×10^9 infectious particles per milliliter can typically be achieved with SAD-B19$^{\Delta G}$, in a period of one to two weeks. CVS-N2c$^{\Delta G}$ titers used here were usually two orders of magnitude lower and generation of concentrated stocks of the virus can take four to six weeks. Given that full-length CVS-N2c can be grown in laboratory to similar titers as SAD-B19, it is possible that future refinement of CVS-N2c$^{\Delta G}$ packaging cells will improve attainable titers to the same level as SAD-B19$^{\Delta G}$.

Our findings therefore establish CVS-N2c$^{\Delta G}$ as an efficient monosynaptic retrograde reagent, one which overcomes many of the drawbacks inherent in the use of SAD-B19-based strains. Additionally, the enhanced ability of functional CVS-N2c$^{\Delta G}$ variants to monitor and manipulate presynaptic neuronal populations may also make it easier to link the organization of neural circuits to their encoded behaviors.

Experimental Procedures

Rescue of CVS-N2c$^{\Delta G}$ variants

DNA rescue plasmids for CVS-N2c were created previously (Wirblich and Schnell, 2011). Four sequence differences were noted for CVS-N2c$^{\Delta G}$ relative to previously published sequences (GenBank HM535790), though we have not explored whether these changes are new mutations or represent historical sequencing errors. Rescue plasmids for deletion mutant CVS-N2c$^{\Delta G}$-insert variants were created by removing the G-gene sequence and introducing 5′ XmaI and 3′ NheI restriction sites and subsequent ligation with expression inserts, while maintaining the entire ~500bp G-L intergenic sequence, with the goal of preserving native viral expression levels and tropism. Removal of the G-L intergenic sequence in a mCherry-expressing variant did not noticeably change the level or pattern of fluorescent protein expression in culture (data not shown). Two fluorescent protein expression inserts were initially constructed, expressing either GFP or dsRed. Rescue was performed in Neuro2A cells (ATCC CCL-131) by co-transfection (Lipofectamine 2000) of CVS-N2c$^{\Delta G}$ genomic plasmid, pCAGGS-T7, pTIT-L, pTIT-N-, pTIT-P (Finke et al., 2003), pCAGGS-N2c(G). Although pTIT helper plasmids correspond to SAD-B19 sequences, their use in only the very first round of rescue minimized genetic drift of CVS-N2c$^{\Delta G}$. pCAGGS-N2c(G) was created by insertion of the N2c glycoprotein gene into the pCAGGS expression plasmid. Rescue took up to 10 days, significantly longer than SAD-B19$^{\Delta G}$. Supernatants from rescue cultures were collected for up to 10 days following the first appearance of virus. It is possible that more efficient RABV backbone plasmids could avoid the use of T7 (Ghanem et al., 2012), but here we found that T7 polymerase was causal to the rescue. All culture of Neuro2A cells and derived lines took place in EMEM with 10% FBS without antibiotics. Cells were grown at 37C and 5% CO_2 until confluent, then held in extended harvesting conditions at 34C and 3% CO_2. Harvested supernatant was filtered at 0.45um and stored at −80°C until used.

Packaging of CVS-N2c$^{\Delta G}$

We considered that maintenance of the virus exclusively in murine neural tissue is likely important to the thousand-fold improvement in neurotropism of the CVS-N2c strain compared to SAD-B19. Neuro2A cells stably expressing either N2c(G) or EnvA_cytG were created for viral amplification and pseudotyping (Figure 1B,C). The resulting cell lines are called N2A-N2c(G) and N2A-EnvA_cytG. For each variant, the glycoprotein gene was cloned into the MLV expression vector pCMMP-IRES-GFP, transfected into Gryphon retroviral packaging cells (Allele Biotech), and MLV-N2c(G)-IRES-GFP after filtering was used to infect Neuro2A cells. We found that Neuro2A cells are significantly less vital in culture than the traditional viral production cell line, BHK-21. Due to their limited vitality, we continued selection of these cells via FACS for more than 6 months. While titers produced are now useful for experimental purposes, they are still at least 2 orders of magnitude lower than titers produced from BHK-21 cells. However, the N2A-N2c(G) packaging line makes up much of the difference in viral counts by increasing effective titer likely due to improved neurotropism. Neuro2A cells expressing EnvA_cytG were created similarly, from a chimeric protein made from EnvA and the tail of N2c(G). Cross-pseudotyping (using EnvA_B19 to pseudotype CVS-N2c$^{\Delta G}$) yielded very low titer,

suggesting that the interaction of C-terminal glycoprotein and RABV M protein is critical for proper packaging.

Amplification was performed by adding rescue supernatant to N2A-N2c(G) cells. Due to the relatively slow metabolism of cells in these conditions, we found it necessary to collect subsequent viral supernatants for up to 28 days in modified culture conditions of 34C and 3% CO_2. Virus for injection was spin purified by ultracentrifugation (2 hour, 20000 RPM) and resuspension of viral pellets in phosphate buffered saline. Pseudotyping was performed by adding amplified supernatant to N2A-EnvA-cytG cells. This was done at the highest possible multiplicity-of-infection (MOI), but typically only 0.20. As noted above, our CVS-N2c$^{\Delta G}$ titers (approximately 10^8 per ml) are orders-of-magnitude lower than what we obtained for SAD-B19$^{\Delta G}$. The resultant virus only infects cells which express the avian TVA receptor, as tested using HEK293-TVA cells (Osakada et al., 2011) and, as designed, does not infect Neuro2A or HEK-293 cells (Figure 1C).

All SAD-B19$^{\Delta G}$ variants were rescued and amplified per standard protocol (Wickersham et al., 2010). Rescue plasmids were constructed from the “Supercut” rescue plasmid (Ghanem et al., 2012). Titers assayed by fluorescent foci were 10^9 – 10^{10} for native-enveloped and 10^8–10^9 for EnvA-pseudotyped.

Testing specificity of viral infection and expression

To test the selectivity of our AAV construct we injected AAV driving the Cre-dependent expression of N2c glycoprotein into the spinal cord of wild-type animals. 1 μl of the AAV-FLEX-nGFP-2A-RABV[G] was injected into the ventral horn at spinal segments L3–L6. Animals were sacrificed after two weeks and the spinal cords assayed for GFP expression. To test for contaminating wild-coat virions in our EnvA-pseudotyped CVS-N2c$^{\Delta G}$ preparations we injected 1.2 μl of these viruses into the ventral horn of spinal segments L3–L6. After 10 days animals were sacrificed and examined for expression of fluorescent protein.

Analysis of Spread

Mice expressing *Adora2a*-Cre (RRID: MMRRC_031168-UCD; Aged 12 to 16 weeks) were used for corticostriatal tracing. Mice expressing *ChAT*-Cre (RRID: IMSR_JAX:006410) were used for spino-motor neuron tracing. For all injections, animals were anesthetized using isoflurane and given analgesics. For corticostriatal injections, a craniotomy was created above dorsal striatum and injection pipette was lowered to target (0.75 mm AP, 2.2 mm ML, 3.3 mm DV). For AAV, we injected 39 nL of a 1:2 cocktail of AAV-FLEX-TVA_mCherry with AAV-FLEX-nGFP-2A-RABV[G]. Following two weeks of recovery and AAV expression, a secondary surgery was performed by the same technique and 300 nL of RABV$^{\Delta G}$(EnvA) was injected. All AAVs were serotyped 2+1, using established procedures (McClure et al., 2011). Pairs of animals were sacrificed at 5, 10, and 15 days following RABV$^{\Delta G}$ infection, brains harvested and sliced at 100 μm by microtome for visualization. There was no significant difference in viral spread over the three differing infection periods. Imaging was done by confocal microscopy (Leica SP5 for corticostriatal, Zeiss 710 for spinal cord). All sections containing priming infection were imaged and

double-labeled cells counted. Additionally, the locus and extent of priming infection was verified as the same, ±100μm, for all six animals. For secondary labeling, slices at 5 AP coordinates (Bregma +2.8, +2.1, +0.5, +0.1, −0.2) were viewed and dsRed+ cells in cortex manually counted.

For analysis of viral spread within the spinal cord, procedures were followed as above, but instead of craniotomy, injections were made into the ventral horn of the cord between L3 and L4 of 12 week old *ChAT*-Cre mice. All secondary labeling was counted within lumbar, thoracic and cervical spinal cord as well as the hindbrain (defined as caudal to Bregma −5.4) (Franklin and Paxinos, 2013).

Gene expression analysis and cytotoxicity

Neuro2A cells were infected with either SAD-B19 or CVS-N2c strains of RABV$^{\Delta G}$-GFP. For immunocytochemical analysis, Neuro2As were cultured in poly-l-lysine coated Labtek chamber slides and fixed with 4% paraformaldehyde in phosphate buffer after 2 or 4 days. Cultures were counterstained with neurotrace-647 (Invitrogen) and mounted in moviol. Images of infected and uninfected cells were taken using a Zeiss 510 confocal microscope with identical settings for each culture. In each field of view the mean grey scale value for infected and uninfected cells was calculated, with uninfected cell values subtracted from infected as background values. Each culture was repeated 3 times with >50 cells analyzed per condition. Culture conditions were identical for analysis of propidium iodide incorporation. After fixation, cells were treated with 100 μg/ml RNAse for 20 minutes at 37°C before addition of 500 nM propidium iodide for 3 minutes at room temperature.

Tissue preparation for *in vitro* electrophysiological recordings

Following surgical procedures above, C57 wild-type mice were infected with SAD-B19 or CVS-N2c strains of RABV$^{\Delta G}$-hChR2-YFP. Six – 10 and 14 days after virus injection we prepared coronal slices (350 μm) from the forebrain containing the injection sites, as described previously (Turi et al., 2015). During recording slices were maintained at room temperature and perfused at 1–2 ml per minute with artificial cerebrospinal fluid (ACSF) containing (in mM) 125 NaCl, 25 $NaHCO_3$, 3 KCl, 1.25 NaH_2PO_4, 1 $MgCl_2$, 2 $CaCl_2$, 22.5 glucose, 3 sodium pyruvate and 1 ascorbate, and saturated with 95% O_2 and 5% CO_2. Slices were visualized with Dodt contrast optics using a Zeiss Examiner Z1 upright microscope equipped with a 63× objective (1.0 NA; Zeiss) and two-photon scanning apparatus (Bruker Technologies).

In vitro electrophysiological recordings and hChR2 photostimulation

For whole-cell current-clamp recordings we patched hChR2 expressing neurons in the secondary motor and cingulate cortices. The intracellular signals were amplified by a Dagan BVC-700A amplifier. Recording pipettes were pulled from borosilicate glass to tip resistances of ~4–7 MΩ and filled with intracellular solution containing low Cl^- (in mM): 140 potassium gluconate, 4 NaCl, 10 HEPES, 4 Mg_2ATP, 0.3 $Tris_2GTP$, 14 phosphocreatine and 0.1 Alexa 594. Pipette capacitance was compensated, and the signals were filtered at 1–10 kHz and digitized at 50 kHz. hChR2 photostimulation was performed with a blue DPSS laser (473 nm, CrystaLaser) coupled to the microscope's two-photon

scan-head (Lovett-Barron et al., 2012). For testing the efficacy of the hChR2 expression we run a 5 Hz photostimulation protocol on the cells held at their resting membrane potential. After recording of 5–8 traces the number of photostimulation evoked spikes was divided by the number of the light stimuli.

Hippocampal window implant

Following surgical procedures above, C57 wild-type mice were infected in the medial septum with SAD-B19 or CVS-N2c strains of RABV$^{\Delta G}$-GCaMP6f. Hippocampal window implant surgeries were performed as described previously (Kaifosh et al., 2013, Lovett-Barron et al., 2014). Briefly, we anesthetized mice with isoflurane and treated them with buprenorphine (0.1 mg/kg, subcutaneous) to minimize postoperative discomfort. We exposed the skull and drilled a 3-mm diameter circle centered over left dorsal CA1, matching the size of the cannula window to be implanted. We removed the bone and dura, and then slowly aspirated cortex covering the hippocampus while constantly irrigating with chilled cortex buffer until the external capsule was exposed. Then we implanted the sterilized window implant by wedging it into place, and secured the top of the cannula to the skull and stainless steel head-post with grip cement, leaving it to dry for 15–20 min before returning mice to the home cage (awake and mobile in 5–20 min). We monitored mice every 12 hours for three days after surgery, administering buprenorphine to minimize any signs of discomfort. Three days after the surgery the animals were habituated to handling and head-fixation then we started to image the GCaMP6f expressing cells.

In vivo cytotoxicity and blebbing analysis

Following injection of SAD-B19 or CVS-N2c strains of RABV$^{\Delta G}$-GCaMP6f into the medial septum, or RABV$^{\Delta G}$-hChR2-YFP into striatum to retrogradely infect corticostriatal neurons, we selected regions with similar numbers of infected neurons for analysis (n = 3 animals per condition; 10–15 neurons analyzed per region for hChR2; 2–10 neurons for GCaMP6f). Identical magnification were used for each sample and the number of blebs were counted for each infected neuron.

Two-photon imaging

We use an *in vivo* a resonant galvo based imaging system (Bruker) and an ultra-fast pulsed laser beam (Coherent; 920-nm wavelength) controlled with an electro-optical modulator to excite GCaMP6f through a 40× objective. Distilled water served to connect the water immersion objective with the cannula. Fluorescent light was detected with photomultiplier tube (green GCaMP6f fluorescence, GaAsP PMT) operated with PrairieView software. In vivo imaging was performed in head-fixed mice running on a linear treadmill (Kaifosh et al., 2013). We tracked locomotor behavior by measuring treadmill wheel rotation, recorded as changes in voltage across an infrared photo-transistor as wheel spokes blocked light from an infrared LED. Time series were collected in green (GCaMP6f signal) channel at 512 × 512 at ~30 Hz then underwent motion-correction as described in (Kaifosh et al., 2013). Regions of interest (ROIs) were manually drawn over corrected time-series in Image J (NIH), to isolate the somata of cells of interest and the extracted ΔF/F signals were aligned with the running signal.

Conditional Recombination

To analyze germline recombination by CVS-N2c$^{\Delta G}$-FLPo-mCherry we injected 50 nl of virus into the ventral spinal at L3 of RCE-FRT mice (Sousa et al., 2009). These animals contain a Frt-flanked STOP cassette prior to the GFP coding sequence, and so report expression of Flp-recombinase. 10 days after CVS-N2c$^{\Delta G}$-FLPo-mCherry injection neurons in the thoracic spinal cord were imaged using a Zeiss 510 confocal microscope and expression of mCherry, GFP or both was noted.

Viral Reagents

CVS-N2c$^{\Delta G}$ RABV and AAV complementation vectors are available from Addgene as Jessell Lab plasmids. Packaging cells (N2A-N2cG, N2A-EnvA_cytG) are available from the authors.

Supplementary Material

Refer to Web version on PubMed Central for supplementary material.

Acknowledgments

We would like to thank E. Callaway (Salk Institute) and I. Wickersham (MIT) for early discussions and the SAD-B19 complementation vector (Addgene 11680). KK Conzelmann (LMU) for SAD-B19 rescue plasmids. A. Sisti for RABV-Cre injections and imaging. S. Fageiry, N. Balaskas, A. Miri and F. Polleux for comments on the manuscript. N. Balaskas and D. Ng for analysis of overlap of motor neuron dendrites. A. Kaufman for technical assistance. I. Schieren for assistance with FACS and imaging. M.S. was supported by the Rabies Core Center grant 5P40OD010996-10. A.L. was supported by McKnight Memory and Cognitive Disorders Award, Human Frontiers Science Program, Brain and Behavior Research Foundation (NARSAD). T.M.J. was supported by NIH grant NS0332245 and Project A.L.S. T.M.J. is a HHMI investigator.

References

Bostan AC, Dum RP, Strick PL. The basal ganglia communicate with the cerebellum. Proc Nat Acad Sci USA. 2010; 107:8452–8456. [PubMed: 20404184]

Callaway EM, Luo L. Monosynaptic Circuit Tracing with Glycoprotein-Deleted Rabies Viruses. J Neurosci. 2015; 35:8979–8985. [PubMed: 26085623]

Cetin A, Callaway EM. Optical control of retrogradely infected neurons using drug-regulated “TLoop” lentiviral vectors. J Neurophys. 2014; 111:2150–2159.

Chen TW, Wardill TJ, Sun Y, Pulver SR, Renninger SL, Baohan A, Schreiter ER, Kerr RA, Orger MB, Jayaraman V, et al. Ultrasensitive fluorescent proteins for imaging neuronal activity. Nature. 2013; 499:295–300. [PubMed: 23868258]

Conzelmann, K.; Hagendorf. Imaging in Neuroscience. CSH Press; 2011. Recombinant Fluorescent Rabies Virus Vectors for Tracing Neurons and Synaptic Connections.

Coulon P, Derbin C, Kucera P, Lafay F, Prehaud C, Flamand A. Invasion of the peripheral nervous systems of adult mice by the CVS strain of rabies virus and its avirulent derivative AvO1. J Virol. 1989; 63:3550–3554. [PubMed: 2664219]

DeNardo LA, Berns DS, DeLoach K, Luo L. Connectivity of mouse somatosensory and prefrontal cortex examined with trans-synaptic tracing. Nat Neurosci. 2015; 18:1687–1697. [PubMed: 26457553]

Dietzschold B, Li J, Faber M, Schnell M. Concepts in the pathogenesis of rabies. Future Virol. 2008; 3(5):481–90. [PubMed: 19578477]

Eccles JC, Eccles RM, Lundberg A. The convergence of monosynaptic excitatory afferents on to many different species of alpha motoneurones. J Physiol. 1957; 137:22–50. [PubMed: 13439582]

Finke S, Conzelmann KK. Replication strategies of rabies virus. Virus Res. 2005; 111:120–131. [PubMed: 15885837]

Finke S, Mueller-Waldeck R, Conzelmann KK. Rabies virus matrix protein regulates the balance of virus transcription and replication. J Gen Virol. 2003; 84:1613–1621. [PubMed: 12771432]

Frank E, Westerfield M. Development of sensory-motor synapses in the spinal cord of the frog. J Physiol. 1983; 343:593–610. [PubMed: 6315924]

Franklin, KBJ.; Paxinos, G. Paxinos and Franklin's The mouse brain in stereotaxic coordinates. Amsterdam: Academic Press, an imprint of Elsevier; 2013.

Gerfen, CR.; Bolam, JP. Handbook of Behavioral Neuroscience. Elsevier; 2010. The Neuroanatomical Organization of the Basal Ganglia; p. 3-28.

Geue L, Schares S, Schnick C, Kliemt J, Beckert A, Freuling C, Conraths FJ, Hoffmann B, Zanoni R, Marston D, et al. Genetic characterisation of attenuated SAD rabies virus strains used for oral vaccination of wildlife. Vaccine. 2008; 26:3227–3235. [PubMed: 18485548]

Ghanem A, Conzelmann K-K. G gene-deficient single-round rabies viruses for neuronal circuit analysis. Virus Res. 2015 In Press.

Ghanem A, Kern A, Conzelmann KK. Significantly improved rescue of rabies virus from cDNA plasmids. Eur J Cell Bio. 2012; 91:10–16. [PubMed: 21397981]

Gong S, Doughty M, Harbaugh CR, Cummins A, Hatten ME, Heintz N, Gerfen CR. Targeting Cre recombinase to specific neuron populations with bacterial artificial chromosome constructs. J Neurosci. 2007; 27:9817–9823. [PubMed: 17855595]

Hongo T, Lundberg A, Phillips CG, Thompson RF. The pattern of monosynaptic Ia-connections to hindlimb motor nuclei in the baboon: a comparison with the cat. Proc R Soc Lond B Biol Sci. 1984; 221:261–289. [PubMed: 6146138]

Hoshi E, Tremblay L, Féger J, Carras PL, Strick PL. The cerebellum communicates with the basal ganglia. Nat Neurosci. 2005; 8:1491–1493. [PubMed: 16205719]

Jackson, AC. Rabies: scientific basis of the disease and its management. Amsterdam; Boston: Elsevier/ Academic Press; 2013.

Jinno S, Klausberger T, Marton LF, Dalezios Y, Roberts JDB, Fuentealba P, Bushong EA, Henze D, Buzsaki G, Somogyi P. Neuronal Diversity in GABAergic Long-Range Projections from the Hippocampus. J Neurosci. 2007; 27:8790–8804. [PubMed: 17699661]

Kaifosh P, Lovett-Barron M, Turi GF, Reardon TR, Losonczy A. Septo-hippocampal GABAergic signaling across multiple modalities in awake mice. Nat Neurosci. 2013; 16:1182–1184. [PubMed: 23912949]

Kanda T, Sullivan KF, Wahl GM. Histone-GFP fusion protein enables sensitive analysis of chromosome dynamics in living mammalian cells. Curr Biol. 1998; 8:377–385. [PubMed: 9545195]

Kelly RM, Strick PL. Rabies as a transneuronal tracer of circuits in the central nervous system. J Neurosci Methods. 2000; 103:63–71. [PubMed: 11074096]

Kiritani T, Wickersham IR, Seung HS, Shepherd GMG. Hierarchical Connectivity and Connection-Specific Dynamics in the Corticospinal-Corticostriatal Microcircuit in Mouse Motor Cortex. J Neurosci. 2012; 32:4992–5001. [PubMed: 22492054]

Klausberger T, Somogyi P. Neuronal Diversity and Temporal Dynamics: The Unity of Hippocampal Circuit Operations. Science. 2008; 321:53–57. [PubMed: 18599766]

Lin JY. A user's guide to channelrhodopsin variants: features, limitations and future developments. Exp Physiol. 2011; 96:19–25. [PubMed: 20621963]

Lovett-Barron M, Turi GF, Kaifosh P, Lee PH, Bolze F, Sun XH, Nicoud JF, Zemelman BV, Sternson SM, Losonczy A. Regulation of neuronal input transformations by tunable dendritic inhibition. Nat Neurosci. 2012; 15:423–430. [PubMed: 22246433]

Lovett-Barron M, Kaifosh P, Kheirbek MA, Danielson N, Zaremba JD, Reardon TR, Turi GF, Hen R, Zemelman BV, Losonczy A. Dendritic Inhibition in the Hippocampus Supports Fear Learning. Science. 2014; 343:857–863. [PubMed: 24558155]

McClure C, Cole KLH, Wulff P, Klugmann M, Murray AJ. Production and Titering of Recombinant Adeno-associated Viral Vectors. J Vis Exp. 2011; 27:e3348. [PubMed: 22143312]

Mebatsion T, König M, Conzelmann KK. Budding of Rabies Virus Particles in the Absence of the Spike Glycoprotein. Cell. 1996; 84:941–951. [PubMed: 8601317]

Mendelsohn AI, Simon CM, Abbott LF, Mentis GZ, Jessell TM. Activity Regulates the Incidence of Heteronymous Sensory-Motor Connections. Neuron. 87:111–123. [PubMed: 26094608]

Mori T, Morimoto K. Rabies virus glycoprotein variants display different patterns in rabies monosynaptic tracing. Front Neuroanat. 2014; 7:47. [PubMed: 24427117]

Morimoto K, Hooper DC, Carbaugh H, Fu ZF, Koprowski H, Dietzschold B. Rabies virus quasispecies: Implications for pathogenesis. Proc Nat Acad Sci USA. 1998; 95:3152–3156. [PubMed: 9501231]

Morimoto K, Hooper DC, Spitsin S, Koprowski H, Dietzschold B. Pathogenicity of different rabies virus variants inversely correlates with apoptosis and rabies virus glycoprotein expression in infected primary neuron cultures. J Virol. 1999; 73:510–518. [PubMed: 9847357]

Morimoto K, Foley HD, McGettigan JP, Schnell MJ, Dietzschold B. Reinvestigation of the role of the rabies virus glycoprotein in viral pathogenesis using a reverse genetics approach. J Neurovirol. 2000; 6:373–381. [PubMed: 11031690]

Namburi P, Beyeler A, Yorozu S, Calhoon GG, Halbert SA, Wichmann R, Holden SS, Mertens KL, Anahtar M, Felix-Ortiz AC, et al. A circuit mechanism for differentiating positive and negative associations. Nature. 2015; 520:675–678. [PubMed: 25925480]

Nassi JJ, Cepko CL, Born RT, Beier KT. Neuroanatomy goes viral! Front Neuroanat. 2015; 9:80. [PubMed: 26190977]

Ogawa SK, Cohen JY, Hwang D, Uchida N, Watabe-Uchida M. Organization of monosynaptic inputs to the serotonin and dopamine neuromodulatory systems. Cell Rep. 2014; 8:1105–1118. [PubMed: 25108805]

Osakada F, Mori T, Cetin AH, Marshel JH, Virgen B, Callaway EM. New Rabies Virus Variants for Monitoring and Manipulating Activity and Gene Expression in Defined Neural Circuits. Neuron. 2011; 71:617–631. [PubMed: 21867879]

Palusa S, Ndaluka C, Bowen RA, Wilusz CJ, Wilusz J. The 3′ untranslated region of the rabies virus glycoprotein mRNA specifically interacts with cellular PCBP2 protein and promotes transcript stability. PLoS ONE. 2012; 7:e33561. [PubMed: 22438951]

Pollak Dorocic I, Fürth D, Xuan Y, Johansson Y, Pozzi L, Silberberg G, Carlén M, Meletis K. A whole-brain atlas of inputs to seretonergic neurons of the dorsal and median raphe nuclei. Neuron. 2014; 83:663–678. [PubMed: 25102561]

Rancz EA, Franks KM, Schwarz MK, Pichler B, Schaefer AT, Margrie TW. Transfection via whole-cell recording in vivo: bridging single-cell physiology, genetics and connectomics. Nat Neurosci. 2011; 14:527–532. [PubMed: 21336272]

Roy A, Hooper DC. Immune evasion by rabies viruses through the maintenance of blood-brain barrier integrity. J Neurovirol. 2008; 14:401–411. [PubMed: 19016377]

Schnell MJ, Mebatsion T, Conzelmann KK. Infectious rabies viruses from cloned cDNA. EMBO J. 1994; 13:4195–4203. [PubMed: 7925265]

Schnell MJ, McGettigan JP, Wirblich C, Papaneri A. The cell biology of rabies virus: using stealth to reach the brain. Nat Rev Microbiol. 2009; 8:51–61. [PubMed: 19946287]

Scott CA, Rossiter JP, Andrew RD, Jackson AC. Structural abnormalities in neurons are sufficient to explain the clinical disease and fatal outcome of experimental rabies in yellow fluorescent protein-expressing transgenic mice. J Virol. 2008; 82:513–521. [PubMed: 17942540]

Sousa VH, Miyoshi G, Hjerling-Leffler J, Karayannis T, Fishell G. Characterization of Nkx6-2-Derived Neocortical Interneuron Lineages. Cereb Cortex. 2009; 19:i1–i10. [PubMed: 19363146]

Sun Y, Nquyen AQ, Nquyen JP, Le L, Saur D, Choi J, Callaway EM, Xu X. Cell-Type-Specific Circuit Connectivity of Hippocampal CA1 Revealed through Cre-Dependent Rabies Tracing. Cell Rep. 2014; 7:269–280. [PubMed: 24656815]

Turi GF, Wittmann G, Lechan RM, Losonczy A. Ambient GABA modulates septo-hippocampal inhibitory terminals via presynaptic GABAb receptors. Neuropharmacol. 2015; 88:55–62.

Ugolini G. Specificity of rabies virus as a transneuronal tracer of motor networks: Transfer from hypoglossal motoneurons to connected second-order and higher order central nervous system cell groups. J Comp Neurol. 1995; 356:457–480. [PubMed: 7642806]

Ugolini G. Advances in viral transneuronal tracing. J Neurosci Meth. 2010; 194:2–20.

Vélez-Fort M, Rousseau CV, Niedworok CJ, Wickersham IR, Rancz EA, Brown APY, Strom M, Margrie TW. The Stimulus Selectivity and Connectivity of Layer Six Principal Cells Reveals Cortical Microcircuits Underlying Visual Processing. Neuron. 2014; 83:1431–1443. [PubMed: 25175879]

Watabe-Uchida M, Zhu L, Ogawa SK, Vamanrao A, Uchida N. Whole-Brain Mapping of Direct Inputs to Midbrain Dopamine Neurons. Neuron. 2012; 74:858–873. [PubMed: 22681690]

Wertz A, Trenholm S, Yonehara K, Hillier D, Raics Z, Leinweber M, Szalay G, Ghanem A, Keller G, Rózsa B, Conzelmann KK, Roska B. Single-cell-initiated monosynaptic tracing reveals layer-specific cortical network modules. Science. 2015; 349:70–74. [PubMed: 26138975]

Wickersham IR, Finke S, Conzelmann KK, Callaway EM. Retrograde neuronal tracing with a deletion-mutant rabies virus. Nat Meth. 2007a; 4:47–49.

Wickersham IR, Lyon DC, Barnard RJO, Mori T, Finke S, Conzelmann KK, Young JAT, Callaway EM. Monosynaptic Restriction of Transsynaptic Tracing from Single, Genetically Targeted Neurons. Neuron. 2007b; 53:639–647. [PubMed: 17329205]

Wickersham IR, Sullivan HA, Seung HS. Production of glycoprotein-deleted rabies viruses for monosynaptic tracing and high-level gene expression in neurons. Nat Protoc. 2010; 5:595–606. [PubMed: 20203674]

Wirblich C, Schnell MJ. Rabies Virus (RV) Glycoprotein Expression Levels Are Not Critical for Pathogenicity of RV. J Virol. 2011; 85:697–704. [PubMed: 21068252]

Zampieri N, Jessell TM, Murray AJ. Mapping Sensory Circuits by Anterograde Transsynaptic Transfer of Recombinant Rabies Virus. Neuron. 2014; 81:766–778. [PubMed: 24486087]

Zhang F, Wang LP, Boyden ES, Deisseroth K. Channelrhodopsin-2 and optical control of excitable cells. Nat Meth. 2006; 3:785–792.

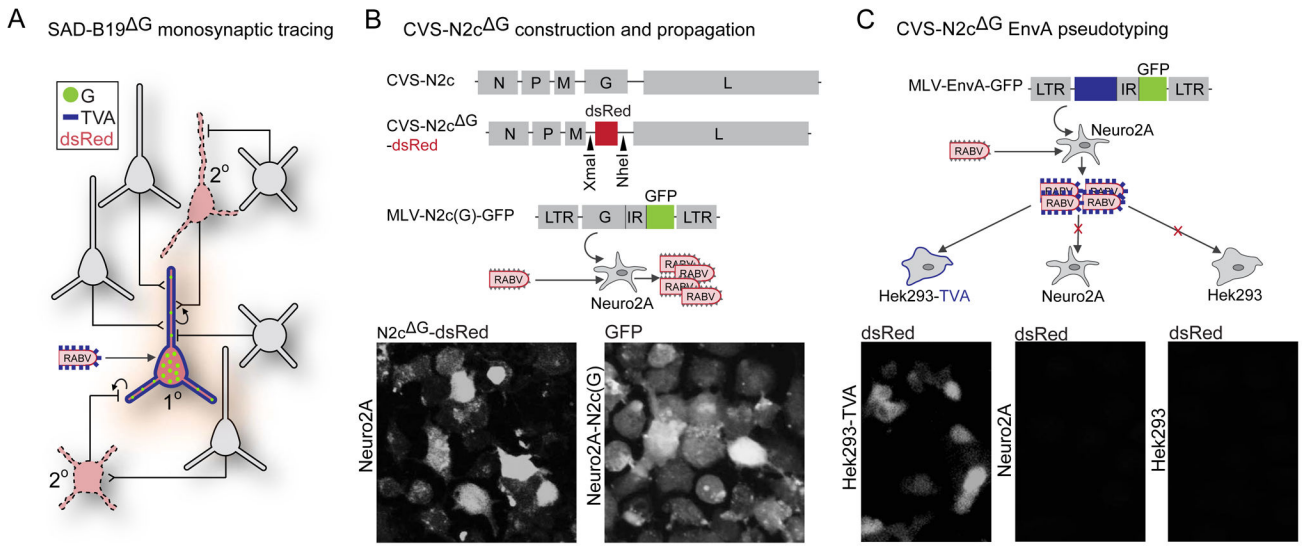

FIGURE 1. Construction and Packaging of CVS-N2c$^{\Delta G}$ for monosynaptic tracing

The CVS-N2c deletion mutant was created in the manner pioneered by Wickersham et al (2007a,b). A key difference is the use of a neural cell line for viral packaging. **(A)** Schematic illustrating monosynaptic restriction of viral spread from starter to secondary neurons. **(B)** CVS-N2c genome and recombinant CVS-N2c$^{\Delta G}$ vector with XmaI/NheI insert restriction sites flanking dsRed insert as well as rescued virus expressing dsRed in Neuro2A cells (top) and complementation vector expressing CVS-N2c glycoprotein inside murine leukosis virus (MLV) (middle) stably transfected into Neuro2A cells for amplification of virus CVS-N2c$^{\Delta G}$ to create the line Neuro2A-N2c(G). Levels of GFP expression correspond to expression of N2c(G) (bottom). **(C)** Complementation vector expressing a chimeric EnvA glycoprotein with short CVS glycoprotein tail (top) transfected into Neuro2A cells for packaging of pseudotyped virus. 293-TVA cells show infection by EnvA-pseudotyped CVS-N2c$^{\Delta G}$ and Neuro2A and Hek293 cells lacking the TVA receptor show no infection by the same virus (bottom).

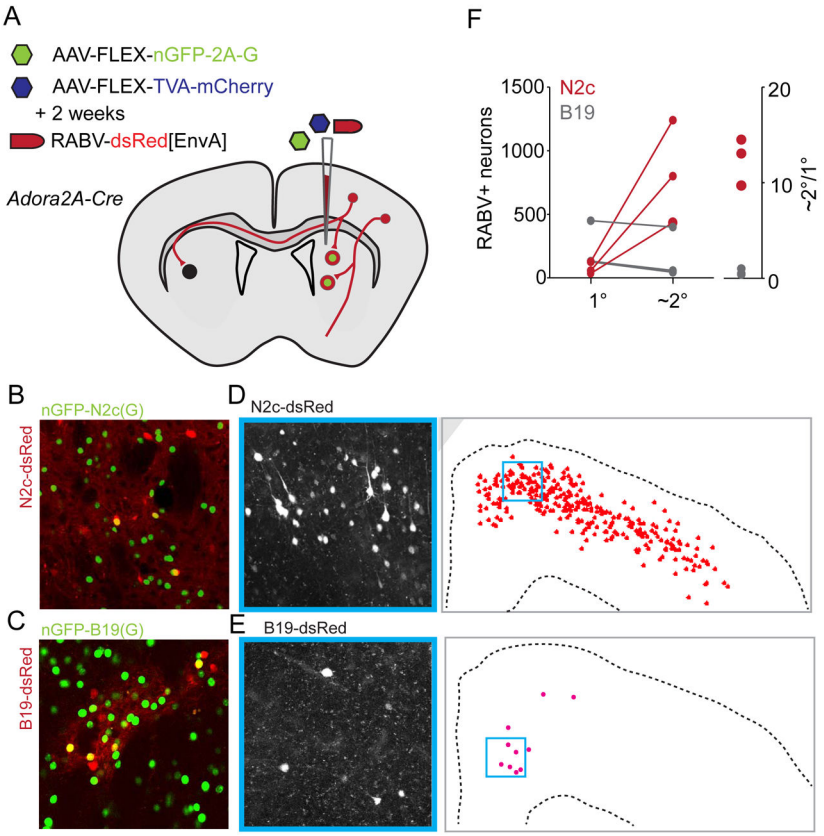

FIGURE 2. Greater transsynaptic transfer for CVS-N2c than SAD-B19 in the forebrain

(A) Schematic for corticostriatal retrograde transsynaptic infection. Primary neurons in striatum infected by conditional AAV expressing RABV(G) and nuclear GFP (histone2B-GFP fusion: nGFP) and AAV expressing TVA and mCherry after recombination via germline *Adora2a*-Cre, and re-infected two weeks later by pseudotyped RABV$^{\Delta G}$–dsRed[EnvA]. **(B–C)** Confocal images of primary infection for SAD-B19 and CVS-N2c. Primary cells display both nGFP as well as dsRed. **(D–E)** Representative image of monosynaptic viral spread with 20× confocal image inset from anatomical plot showing all RABV+ neurons. **(F)** Plot of infection spread from primary striatal to secondary cortical neurons in 6 mice, 3 for each viral strain. Primary infection was marked by expression of both dsRed from RABV and nGFP from the AAV complementation vector. Primary infection was constrained to small populations in the same region of anterior dorsal striatum. Secondary infection was calculated by sampling the same 5 coronal sections from each animal as identified by position relative to Bregma. Pan-cortical secondary infection is greater, but scales with numbers shown here.

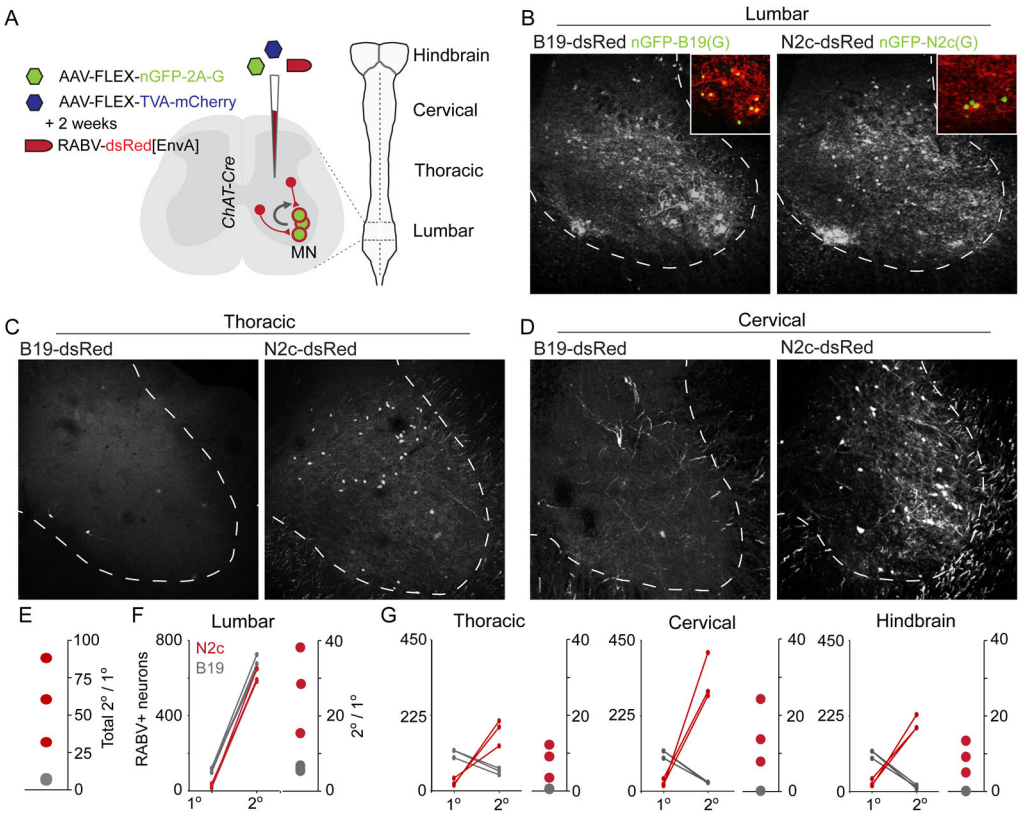

FIGURE 3. CVS-N2c$^{\Delta G}$ from lumbar motor neurons shows enhanced transsynaptic spread compared to SAD-B19$^{\Delta G}$

(A) Schematic of RABV-monosynaptic tracing from lumbar motor neurons. **(B–D)** Representative images for each viral strain showing transsynaptically transferred infection at lumbar **(B)**, thoracic **(C)** and cervical **(D)** levels. **(E)** Total primary to secondary ratios for SAD-B19$^{\Delta G}$ (grey) and CVS-N2c$^{\Delta G}$ (red). **(F,G)** Plot of infection spread from primary to secondary neurons in 6 mice, 3 for each viral strain, at local lumbar **(F)**, and **(G)** distant thoracic, cervical and hindbrain levels.

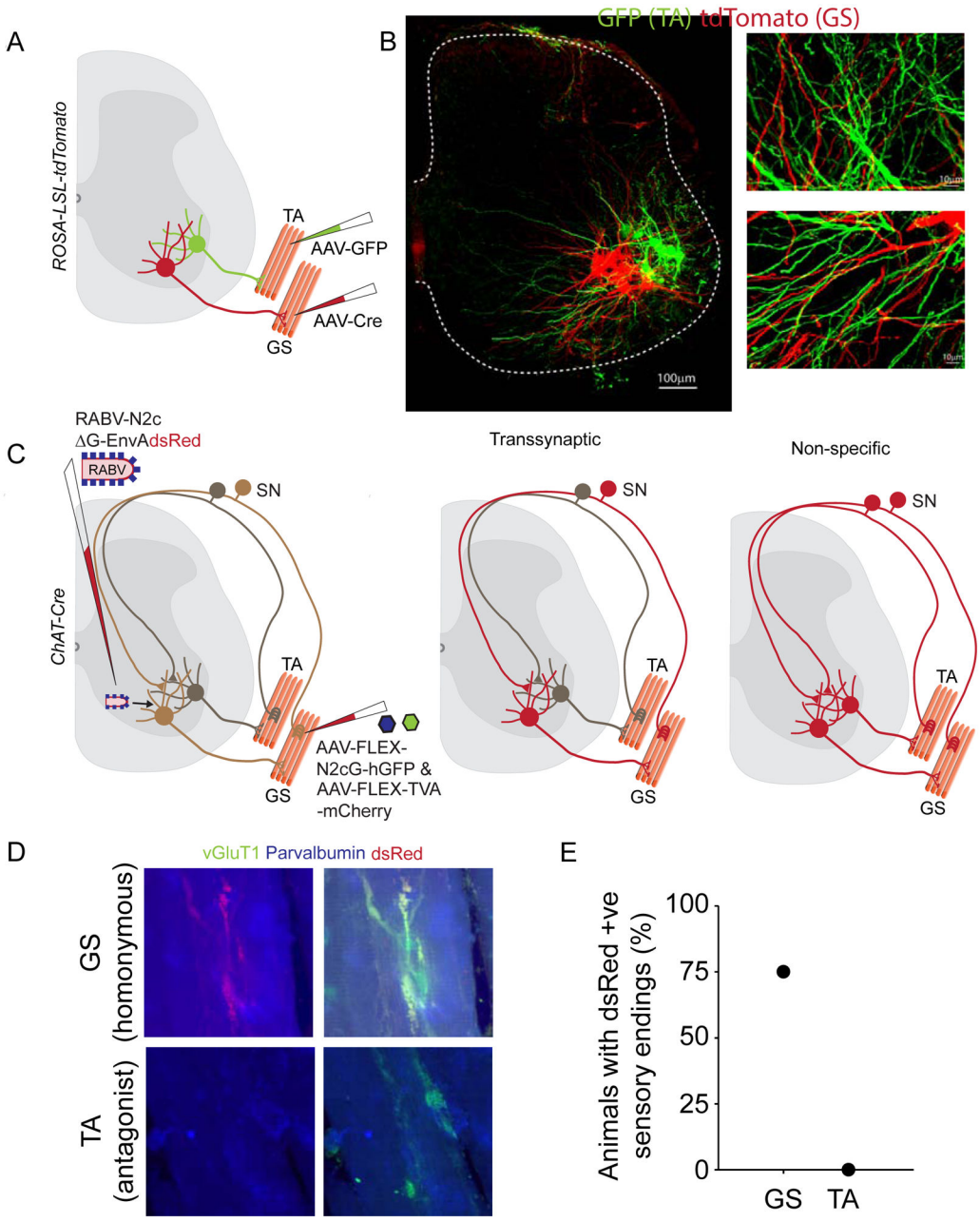

FIGURE 4. Restricted transsynaptic transfer of CVS-N2c$^{\Delta G}$

(A) Experimental design to examine overlap of GS and TA motor neuron dendrites. (B) Fluorescent labeled motor neurons showing overlap of GS and TA dendrites. (C) Assay to test for selective trans-synaptic transfer of RABV. (D) Example images of GS and TA muscle spindles showing dsRed positive sensory endings in GS (top) but not TA (bottom). (E) Quantitation of labeled sensory endings in GS or TA muscles.

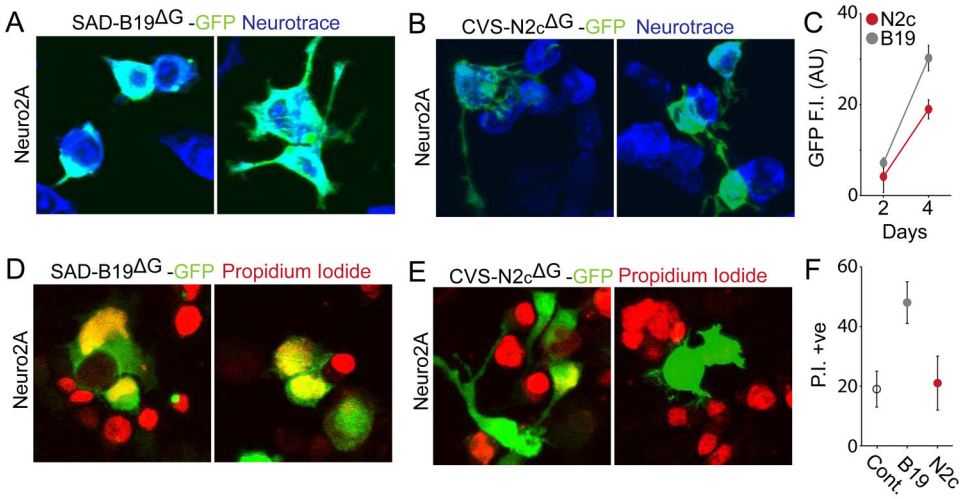

FIGURE 5. Reduced expression level and cytotoxicity of CVS-N2c compared to SAD-B19

(A) Neuro2A cells infected by GFP-expressing SAD-B19$^{\Delta G}$ or **(B)** CVS-N2c$^{\Delta G}$. **(C)** Intensometric plot of GFP expressed by each RABV strain at 2 and 4 days post-infection, normalized to single infected cells. **(D)** Neuro2A cells infected with SAD-B19$^{\Delta G}$ or **(E)** CVS-N2c$^{\Delta G}$ after 4 days and treated with propidium iodide, a proxy marker for cell death at 4 days post-infection. **(F)** Relative cell death after infection by each RABV strain. Error bars in C and F represent ± SEM.

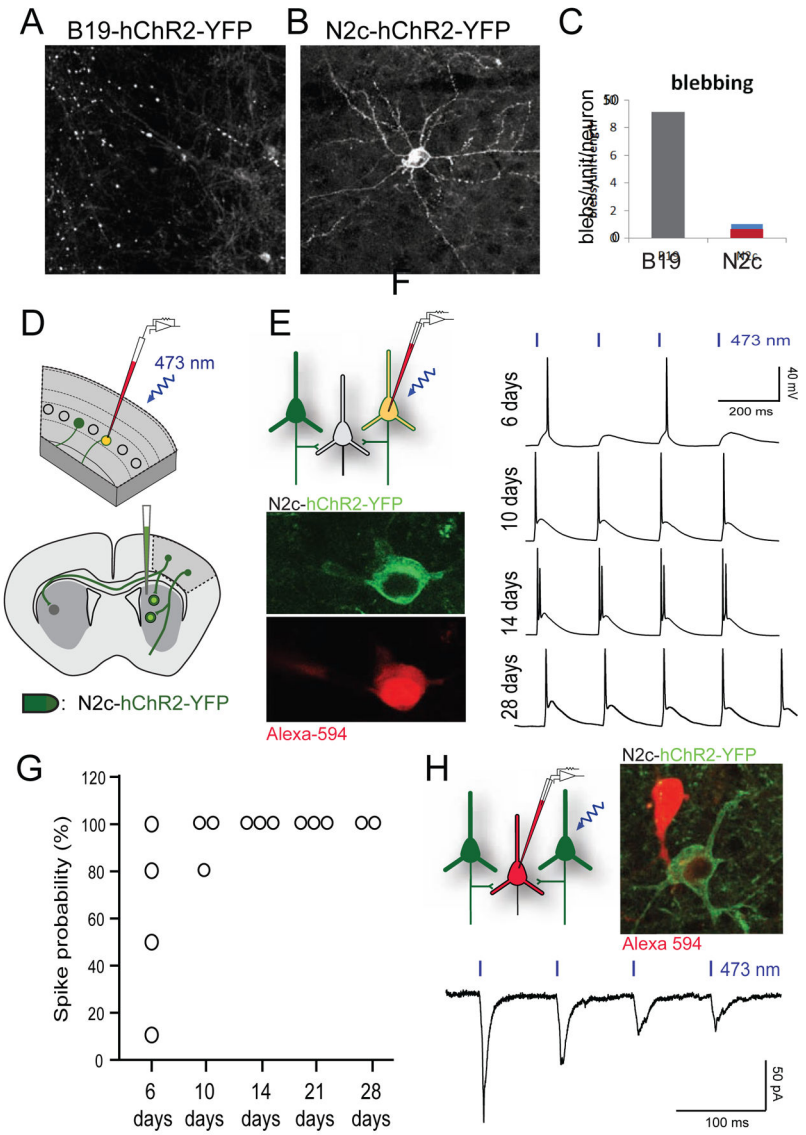

FIGURE 6. CVS-N2c$^{\Delta G}$ is an effective transsynaptic vector for optogenetic manipulation

(A) Confocal image of neurons after 7 days of infection by SAD-B19$^{\Delta G}$ virus expressing hChR2-YFP (cortex). **(B)** Same proteins via virus CVS-N2c$^{\Delta G}$. **(C)** Assay of cell health by morphological irregularity, blebs along proximal dendrites per RABV-infected neuron. **(D)** Schematic of corticostriatal retrograde infection using CVS-N2c$^{\Delta G}$-hChR2-YFP in the dorsal striatum in wild type mice and retrograde spread into cortex (top) and patch-clamp recording of infected cortical neurons (bottom). **(E)** Schematic of whole-cell current-clamp recordings obtained from neurons in acute cortical slices (top). In vitro two-photon images of a recorded cortical neuron retrogradely infected by CVS-N2c$^{\Delta G}$-hChR2-YFP (green) and filled with fluorescent dye from patch pipette (red). **(F)** Example hChR2-photostimulation-evoked voltage responses recorded from CVS-N2c$^{\Delta G}$-hChR2-YFP-infected neurons at 6, 10, 14, and 28 days post infection as seen in (*B*). **(G)** Spike probability at each 6/10/14/21/28 DPI showing increasing effectiveness of hChR2 expressed by the CVS-N2c$^{\Delta G}$ vector. **(H)**

Schematic and *in vitro* two-photon image showing CVS-N2c$^{\Delta G}$-infected (green) neuron in the vicinity of a non-infected cortical neuron filled with red fluorescent dye via patch pipette (top). Example averaged postsynaptic responses recorded from the non-infected neuron confirming effective synaptic release at 8 days post infection (bottom).

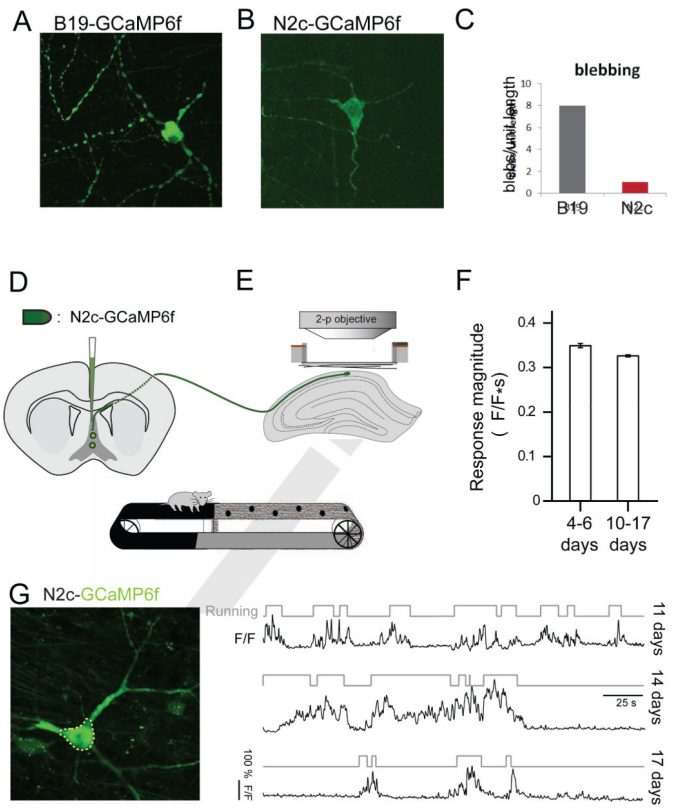

FIGURE 7. CVS-N2c$^{\Delta G}$ is an effective transsynaptic vector for optogenetic monitoring

(A) Confocal image of neurons after 10 days of infection by SAD-B19$^{\Delta G}$ virus expressing GCaMP6f (medial septum). **(B)** Same protein via virus CVS-N2c$^{\Delta G}$. **(C)** Assay of cell health by morphological irregularity, blebs along proximal dendrites per RABV-infection neuron. **(D)** Schematic of infection of CVS-N2c$^{\Delta G}$-GCaMP6f in medial septum and retrograde spread to the dorsal hippocampus. **(E)** Schematic of head-fixed two-photon imaging of dorsal hippocampus of mouse running on an environmentally enriched treadmill (top), *in vivo* two-photon image of an example septal projecting neuron imaged for activity in the area CA1 of the dorsal hippocampus (middle), and time-series of neural activity, expressed as relative changes in GCaMP6f fluorescence (Δ*F*/*F*, black traces) of neuron during running bouts (grey traces) on belt, imaged via *in vivo* two-photon microscopy (bottom). **(F)** Population summary of the magnitude of running-evoked of Ca^{2+} signals indicating comparable responses over extended periods after infection (4–6 DPI: n = 13 cells in n = 2 animal; 10–17 DPI: n = 31 cells in n = 3 animals, Wilcoxon-Mann-Whitney two sample rank test, p = 0.592). **(G)** *In vivo* two-photon image of the same septal-projecting neuron in area CA1 of the dorsal hippocampus (left), and GCaMP6f fluorescence Ca^{2+} signals (Δ*F*/*F*, black traces) recorded from the same neuron during running (grey traces) at 11, 14, and 17 days post-injection (right). Error bars in F represent ± SEM.

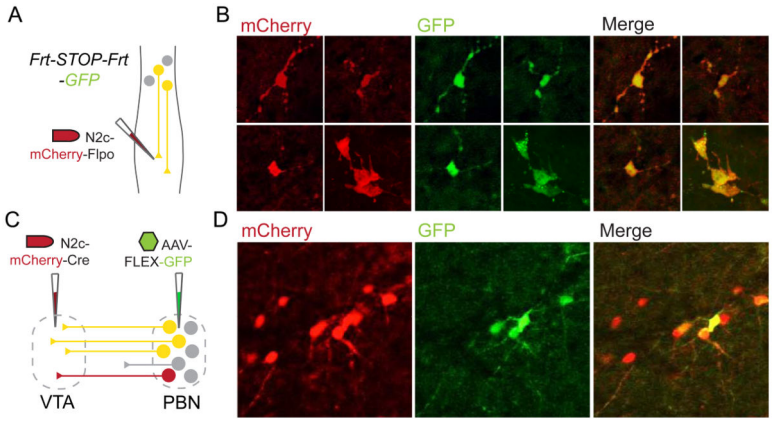

FIGURE 8. CVS-N2c$^{\Delta G}$ drives Cre- or Flp-dependent recombination

(A) Schematic depicting injection of CVS-N2c$^{\Delta G}$-mCherry-Flpo and recombination in Frt-STOP-Frt-GFP mouse line. **(B)** Confocal images of thoracic spinal cord showing recombination in retrogradely infected neurons. **(C)** Schematic depicting injection and recombination by CVS-N2c$^{\Delta G}$-mCherry-Cre. **(D)** Images in parabrachial nucleus (PBN) showing neurons after recombination and expression from a local AAV-FLEX-GFP injection and a corresponding infection in VTA and retrograde uptake of Cre-expressing virus by PBN neurons.

Table 1

Comparison of packaging, titers, expression and application of SAD-B19 $^{\Delta G}$ and CVS-N2c $^{\Delta G}$ RABV strains. See text for further details.

	SAD-B19	**CVS-N2c**
Type	**Vaccination strain**	**Challenge strain**
Packaging		
Native-coat G	Standard cell culture in BHK-21 cells; 7 days production time.	Specialized culture in Neuro2A cells; 28 day production time.
Pseudotyped EnvA	7–10 days for production	14 to 28 days for production.
Complementation	Commercially available viruses, transgenic animals available, requires B19-specific glycoprotein complementation	N2c-specific glycoprotein vectors required, and available. Transgenic animals not yet available.
Titers		
Native-coat G	Low 10^9 typical	Mid 10^7 typical
Pseudotyped EnvA	Low 10^8 typical, native-coat background 10^2 typical	Low 10^7 typical, no detectable native-coat background.
Expression		
Onset	Visible fluorescence within 24 hours.	Requires ≥ 4 days for visible fluorescence.
Specificity	Infects glia, limited reports of retrograde *in vivo* specificity.	No glial infection, demonstrated retrograde *in vivo* specificity.
Toxicity	Modest with fluorophores, higher with optogenetic proteins.	Low with fluorophores; survival up to 28 days even with optogenetic proteins.
Applications		
Transsynaptic Transfer	7–40 presynaptic neurons typical with AAV complementation. Poor transfer to long-range inputs.	60–400 presynaptic neurons. Good transfer to long-range inputs.
Optogenetic manipulation (eg. ChR)	Short-term utility (1–5 days). Toxicity apparent ≥ 5 days.	Medium-term utility (7–28 days longest tested).
Optogenetic monitoring (eg. GCaMP)	Short-term utility (1–10 days). Toxicity apparent ≥ 10 days.	Medium-term utility (7–21 days longest tested).